Oxid Met (2015) 83:441–451
DOI 10.1007/s11085-015-9530-y

ORIGINAL PAPER

First Three-Dimensional Atomic Resolution Investigation of Thermally Grown Oxide on a FeCrAl Alloy

Fang Liu · Mats Halvarsson · Kristina Hellström · Jan-Erik Svensson · Lars-Gunnar Johansson

Received: 9 December 2014 / Revised: 15 January 2015 / Published online: 29 January 2015

Abstract Thermally grown Al_2O_3 scales formed on a FeCrAl alloy, Kanthal APMT, were successfully analysed using pulsed green laser atom probe tomography. The alloy was exposed to 5 vol.% O_2 + 95 vol.% N_2 at 900 °C for 1 h, and covered by a thin layer of Al_2O_3. Cr segregation to some of the Al_2O_3 grain boundaries was observed. The continuous Cr-rich band, which contains a large number of Cr- and/or Fe- enriched nano-sized particles, was studied in detail. Four types of nanoparticles were found and analysed. Oxidation mechanisms at the initial stages are discussed based on the observations.

Keywords Steel · Atom probe tomography · STEM · High temperature corrosion · Segregation

Introduction

FeCrAl alloys provide good high temperature corrosion resistance up to ~1,100 °C, therefore they are widely used in applications, such as heating elements in furnaces, carrier material for catalytic converters for automobiles, and first-walls and blankets in nuclear power plants. There have been extensive studies focusing on understanding the initial stages of high temperature oxidation by using various

F. Liu (✉) · M. Halvarsson
Department of Applied Physics, Chalmers University of Technology, 41296 Göteborg, Sweden
e-mail: fang.liu@chalmers.se

K. Hellström · J.-E. Svensson · L.-G. Johansson
Department of Chemical and Biological Engineering, Chalmers University of Technology, 412 96 Göteborg, Sweden

L.-G. Johansson
High Temperature Corrosion Centre, Chalmers University of Technology, 412 96 Göteborg, Sweden

materials characterization tools: X-ray diffraction (XRD), secondary ion mass spectrometry (SIMS), Auger electron spectroscopy (AES), scanning electron microscopy (SEM), and transmission electron microscopy (TEM) [1–5]. It has been found that after exposure to O_2-containing atmosphere at >800 °C for 1 h, a very thin ($\sim$100 nm) oxide scale is formed. It consists mainly of Al_2O_3 and exhibits a layered structure: a relatively thick outward growing Al_2O_3, a continuous Cr-rich zone close to the oxide/metal interface, and a relatively thin inward growing layer of pure α-Al_2O_3. This microstructure has been reported previously in both wrought and powder metallurgical FeCrAl alloys [1, 6]. However, the techniques been used, i.e. XRD, SIMS, AES, and SEM have a limited lateral resolution. TEM can potentially resolve individual atomic columns [7], however suffering from compressing information along the specimen's thickness direction and projecting three-dimensional information into two-dimensional. A TEM specimen thickness is typically around 100 nm, which is comparable with the thickness of the oxide scale formed at the initial stages. Therefore, quite some details cannot be revealed by TEM.

Atom probe tomography (APT) is the only technique that can provide chemical information with close to atomic resolution ($\sim$0.7 nm) and high chemical sensitivity ($\sim$10 atomic ppm) in three dimensions. In the latest decade it became possible to use APT to study materials with poor electrical conductivity, like oxides, thanks to the new advances, i.e. pulsed-laser aided field evaporation, and sample preparation by combined focused ion beam/scanning electron microscopy (FIB/SEM). Recently, APT has been successfully applied to polycrystalline Al_2O_3 ceramic [8], ZrO_2 [9, 10] and thermally grown Cr_2O_3 on stainless steels [11, 12]. These studies show great potential of applying APT to reveal the corrosion mechanisms of Al_2O_3-forming high-temperature alloys. How to optimize APT operation parameters and some other import issues related to quantitative APT analysis for thermally grown Al_2O_3 have been reported recently [13]. Here we show that APT can provide unique information, which together with information obtained by other techniques can make substantial contribution to a deeper understanding of high temperature oxidation mechanisms.

Materials and Methods

The FeCrAl alloy investigated is Kanthal APMT, with nominal chemical composition (in at%) 22 Cr, 10 Al, 1.6 Mo, 1.2 Si, 0.4 Mn, and trace amount of Y, Zr, Hf, Ti, Mg, S, C, and N (balance Fe). Alloy coupons ($1.5 \times 1.5 \times 0.2$ cm^3) were ground and polished and finished with 1 μm diamond spray. The coupons were then cleaned in ethanol using ultrasonic agitation, and rinsed in acetone and then ethanol. After this they were exposed to 5 vol.% O_2 + 95 vol.% N_2 at 900 °C for 1 h. TEM and APT specimens containing oxide scale and underlying metal were prepared in an FEI Strata Dual Beam 235M workstation, a combined FIB/SEM. In-situ lift-out technique was employed, and the detailed process was reported in ref [14, 15]. The final TEM membrane had a thickness of $\sim$100 nm. TEM/EDS analyses were preformed in a Titan 80-300 TEM. Final APT specimens have a sharp-needle shape with a tip radius <50 nm. An Imago LEAP 3000X HR local

electrode atom probe instrument equipped with a green light (wavelength 532 nm) laser pulsing system was used. The laser pulsing frequency was 200 kHz, and laser energy 0.5 nJ. The chosen target evaporation rate was one ion per 200 pulses. The specimen was kept at 85 K during analyses. The acquired data were reconstructed and further analysed by using the IVAS^{TM} 3.6.2 software developed by CAMECA.

Results

Figure 1 shows a TEM high angle annular dark field (HAADF) micrograph of the oxide scale and underlying metal after 1 h exposure to 5 vol.% O_2 + 95 vol.% N_2 at 900 °C. On top of the oxide is a Pt layer, which was deposited during TEM sample preparation to protect the oxide surface. The contrast in a HAADF image reflects the difference in atomic numbers, the brighter areas having higher atomic numbers, and vice versa. Due to the large difference in atomic numbers, the Pt layer, oxide scale and the alloy substrate are clearly distinguishable.

The oxide scale has a thickness in the range 80–150 nm and exhibits a layered structure. The overall scale structure is similar to that reported previously for this alloy and other FeCrAl alloys oxidized under similar conditions. TEM/EDX analysis shows that the top part (40–80 nm) of the oxide consists of alumina grains, some of which containing Fe, while the bottom layer (10–20 nm) consists of pure alumina. The bright band (20–50 nm) sandwiched between the top and bottom part of the scale is enriched in Cr and occasionally Fe. In addition, Fig. 1 shows several grey scale contrasts that reveal different nano-sized features. The top part of the scale exhibits large (tens of nanometres) regions enriched in Fe that appear bright. Interestingly, the Cr-rich band contains a large number of nano-sized particles that appear bright compared to the surrounding oxide. However, the ~10 nm-sized particles overlap upon each other in the 100 nm thick TEM specimen, making unambiguous analysis of individual particles impossible.

APT analyses revealed these features in detail. Figure 2a shows a reconstruction of an APT dataset that probes a volume containing polycrystalline alumina scale and the underlying alloy, the thickness of the scale being ~120 nm. Only CrO^+ and

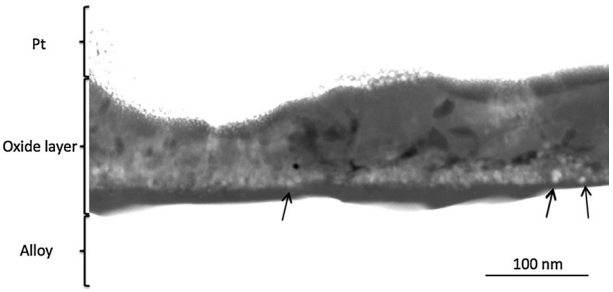

Fig. 1 TEM HAADF micrograph showing the alumina scale and underlying FeCrAl alloy (*bright*) after 1 h at 900 °C in 5vol.%O_2 + 95vol.%N_2. Note the continuous band with *bright* nano-sized particles (some of which are highlighted by *arrows*) close to the metal-oxide interface

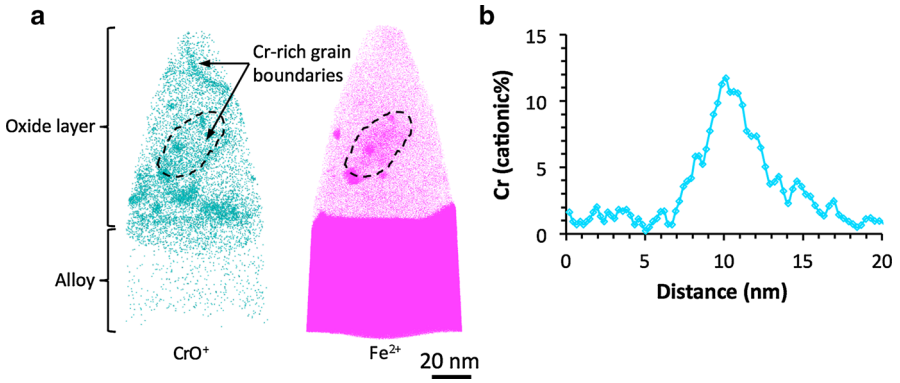

Fig. 2 (colour online) **a** APT reconstruction of a data set obtained from a volume containing the alumina scale and underlying FeCrAl alloy. The light blue and magenta dots represent CrO^+ and Fe^{2+}, respectively. There are two grain boundaries enriched in CrO^+. The reconstruction is aligned in the way that the *upper* boundary appears as a *curve*, and the lower boundary as a *plane* roughly parallel to the paper (the area is indicated by the *dash line*). The *lower* boundary is better illustrated by the cross-section view in Fig. 3a). Note the nano-sized particles enriched in Cr and/or Fe. **b** The Cr concentration profile across the *upper* grain boundary

Fe^{2+} ions are shown in the ion maps to highlight some of the interesting features in the oxide scale:

- Two alumina grain boundaries enriched in Cr, one in the top part of the oxide scale with the boundary plane approximately perpendicular to the image plane, the other in the middle of the oxide scale with the plane of the boundary parallel to the plane of the image.
- An Fe-rich oxide grain (the area inside the dashed line), located on one side of the lower Cr-rich boundary.
- Several Cr- and/or Fe-rich nano-sized particles in the middle and in the bottom of the alumina layer.

The microstructure of these features is described in detail below.

The Cr-Rich Grain Boundaries and the Oxide Grains

As mentioned above, the APT reconstruction in Fig. 2 contains two Cr-rich grain boundaries. The Cr concentration was calculated after background subtraction. A small portion of the ions forming the image in Fig. 2 is background noise collected in the APT during analysis. In general, the background level is higher for analyses of oxides than for metals. The grains separated by the upper boundary consist of almost pure Al_2O_3 with about 0.2 at % Cr (cationic). The maximum Cr concentration along the boundary is 12 at % (cationic). The concentration profile across the grain boundary (Fig. 2b) shows a rather sharp Cr peak, with no obvious tailing into the grain bulk. The second (lower in Fig. 2) grain boundary separates an almost pure alumina grain and an oxide grain with 7.8 at% dissolved Fe (cationic), the balance of

the cations being Al. The maximum concentration of dissolved iron detected by APT in an oxide grain was 16.3 at% (cationic). The Fe analysis of the oxide grains by APT is consistent with TEM/EDX analyses of a large number of oxide grains.

Nano-Sized Particles

The APT reconstruction (Fig. 2) reveals that the nano-sized particles are only present in the middle section of the oxide scale, in consistence with the TEM results (Fig. 1). Four categories of particles can be identified according to their chemical compositions and morphology: spheroid Fe-rich, spheroid Fe- and Cr-rich, spheroid Cr-rich, and irregular-shaped Cr-rich particles. Typical chemical compositions of the four categories are shown in Table 1. Because of the high Fe and Cr content, all four types of nanoparticles appear bright in the HAADF images compared to the Al_2O_3 grain matrix. Many such nanoparticles can be seen in Fig. 1 (a few of them are highlighted by arrows in Fig. 1). It may be noted that the oxygen concentration in the oxide scale, as determined by APT, was round 54 at%, which is below the stoichiometric value (60 at%) for Al_2O_3. The low oxygen analysis is an artefact and the reasons behind it were explored in Ref. [13]. Hence, the particles of type IV (with 54.5 % O (atomic) by APT, see Table 1) correspond to stoichiometric oxide ($(Al,Cr)_2O_3$). Also, it can be concluded that the particles of types I, II and III are not fully oxidized as they consistently exhibit lower oxygen content (Table 1). The lowest oxygen content detected corresponds to 33.1 at % O (type II). Moreover, the type I, II and III particles have spheroid shape and tend to be smaller than the irregular ones (type IV).

Figure 3 displays Fe^{2+} and CrO^{+} ion maps for three cross-sections that are roughly parallel to the oxide/metal interface. The continuous Cr-rich curve in Fig. 3a corresponds to the lower grain boundary shown in Fig. 2. The upper grain in Fig. 3a has very low concentrations of dissolved iron and chromium and contains a Cr-rich spheroid nanoparticle (<10 nm). An Fe-rich nanoparticle is present inside the lower grain, which also contains much dissolved Fe (Fig. 3a). Nanoparticles rich in Fe and Cr are detected along the grain boundary (Fig. 3b). The different types of nanoparticles show distinct distribution patterns. While the spheroidal Cr-rich particles always occur inside alumina grains containing very low amounts of dissolved Fe and Cr (to the upper grain in Fig. 3a), Fe-rich nanoparticles are rare in such alumina grains. Also, the irregular shaped nanoparticles ($(Al,Cr)_2O_3$) are

Table 1 APT analysis results of typical chemical compositions for the four categories of nano-particles (at %)

Particle type	O	Al	Cr	Fe
I Fe-rich	41.4	31.6	1.1	25.9
II Fe-, Cr-rich	33.1	24.5	27.8	14.6
III Cr-rich spheroid	43.4	31.0	25.0	0.6
IV Cr-rich irregular	54.4	28.6	16.4	0.6

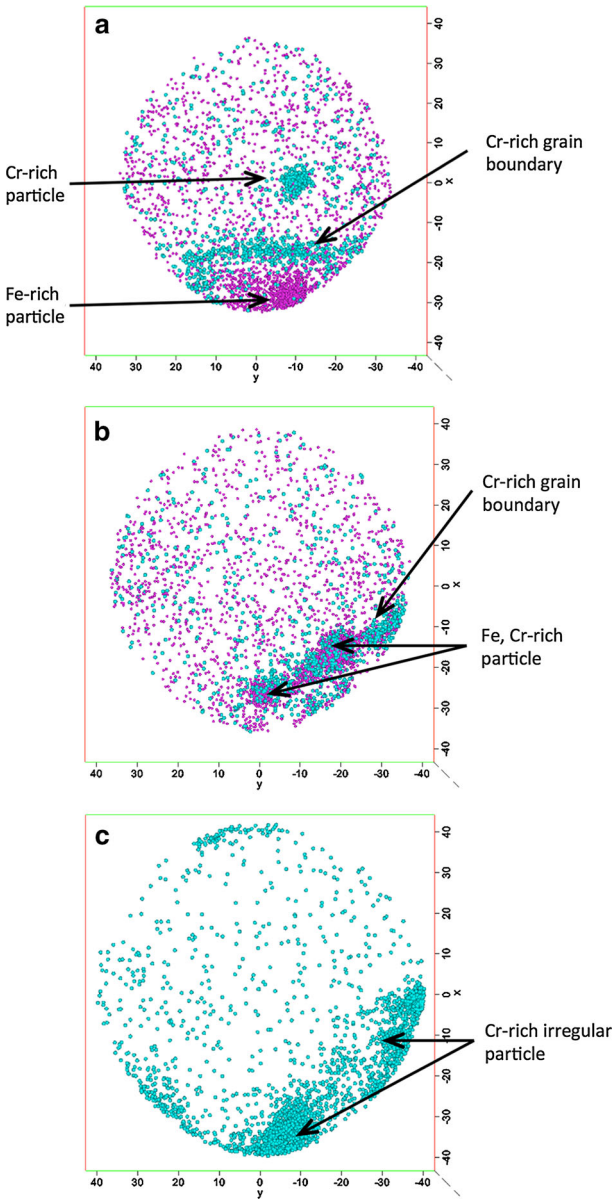

Fig. 3 (colour online) Cross-section view of three thin slices (perpendicular to the analysis axis), showing nano-particles. The light *blue spheres* and *magenta dots* represent CrO^{+} and Fe^{2+}, respectively. **a** An Fe-rich nano-particle inside the Fe-rich Al_2O_3 grain, and a spheroid Cr-rich nano-particle in the neighbouring Al_2O_3 grain. **b** Two Fe- and Cr-rich nano-particles along the oxide grain boundary. **c** Irregular shaped Cr-rich nano-sized particle

located close to the alloy substrate below the spheroidal particles. 1D concentration profiles through the three types of spheroidal and the irregular shaped nano-particles are displayed in Fig. 4a, b, c and d.

Discussion

This paper uses HAADF imaging and APT to analyse the microstructure of the alumina scale formed on the commercial FeCrAl alloy, Kanthal APMT, at 900 °C. While the present results are fully compatible with the previous studies mentioned in the introduction, APT provides a lot of new information in 3D with unparalleled spatial and chemical resolution. Because the volume analysed by APT is quite small (typically 100 × 100 × 150 nm) and contains few alumina grains, there are likely additional scale features, not observed in this study.

The APT analysis adds to the HAADF TEM-EDX analysis in several ways. Both techniques show that the top part of the scale contains both relatively pure alumina grains and grains with a high concentration of dissolved Fe. Also, both methods show that the oxide grains at the alloy interface consist of very pure alumina. The APT analysis reveals that the nanoparticles in the Cr-enriched "band" detected by HAADF (See Fig. 1) are enriched in Cr and/or Fe. The nanoparticles show a lot of diversity and can be categorized into four different types, three of which being substoichiometric with respect to oxygen. One of the salient features in the APT reconstructions is the chromium enrichment in the alumina grain boundaries (Figs. 2, 3) that appears throughout the scale, except for the bottom layer. This is not described in the previous investigations, neither is it detected by HAADF—TEM-EDX.

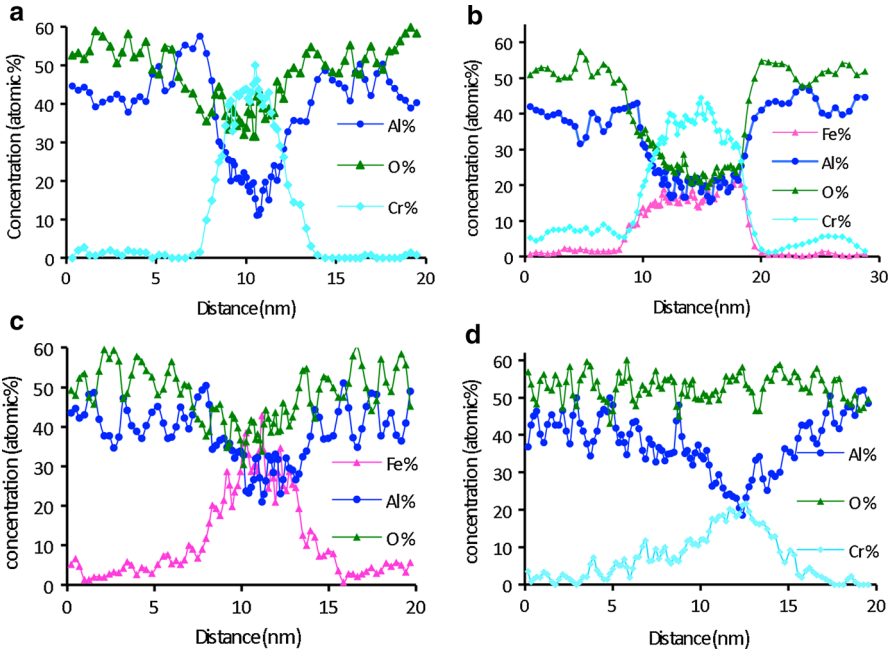

Fig. 4 Concentration profiles through nano-particles. **a** Cr-rich particle; **b** Cr- and Fe-rich particle; **c** Fe-rich particle; **d** irregular-shaped Cr-rich particle

The analysed scale volume shown in Fig. 2 can be described in terms of three layers where the nanoparticles are dispersed in a 50 nm thick slab (corresponding to the Cr-rich band in the HAADF micrograph), which is sandwiched between a 50 nm thick top oxide layer and a 10 nm thick bottom oxide layer. Previous investigations interpreted the Cr enriched band and the Fe in the outer part of the scale as vestiges of transient oxidation [1, 3, 16]. It was hypothesized that during the initial stages of the exposure (including the heat-up) the metal oxidizes indiscriminately, forming a mixture of Fe, Cr and Al oxides. Further it was argued that as oxidation slows down due to scale growth, the great thermodynamic stability of alumina would decrease the oxygen activity at the scale/metal interface enough for the oxidation of Fe and Cr to cease. The continued scale growth would then occur by a Wagner-type mechanism where the reduction of O_2 at the scale surface is coupled to aluminium oxidation by outward transport of metal cations and electrons and inward transport of oxide ions. Thus, the alumina scale situated below the Cr band was thought to consist of inward grown α-Al_2O_3 while the top part of the alumina scale (outside the Cr rich band) was considered to be outward grown.

The present results can be interpreted using this scenario. Accordingly, the Fe and Cr detected in the middle scale layer are considered to have entered the scale during initial, transient oxidation. Also, the very high purity of the bottom alumina layer indicates that it has formed at a later stage, when the oxidation of Fe and Cr has ceased. Conversely, the Fe and Cr ions found in the top part of the scale are considered to have migrated outward and remained there, carrying part of the cationic current. Thus, the top and bottom parts of the scale are considered to consist of inward and outward grown oxide that has formed simultaneously. While the phase composition of the top scale layer has not been established in the present case it is suggested to consist of transient alumina, at least partially. This suggestion is based on a recent paper that reported that the top part of the layered scale formed initially upon oxidation of an FeCrAl alloy at 900 °C, consisted of transient alumina (γ or θ Al_2O_3) [16]. Also, the transient aluminas are known to be cationic conductors and to dissolve high concentrations of divalent ions, (i.e. Fe^{2+}), while trivalent ions (i.e. Cr^{3+}) are much less soluble [17]. This would explain the present observation that in the middle and top part of the scale, Fe ions are dissolved in some of the alumina grains while Cr^{3+} segregates at the grain boundaries (see Fig. 3). Conversely, the pure alumina layer at the bottom of the scale is suggested to consist of α-alumina.

The transition from the initial, rapid and relatively indiscriminate oxidation of an alloy to the formation of a continuous layer of a thermodynamically favoured and slow growing oxide (e.g. α-Al_2O_3) has been suggested to be accompanied by the reduction of less stable oxides in the scale through redox reactions of the type [18]:

$$Cr_2O_3(s) + 2Al(alloy) \rightarrow Al_2O_3(s) + 2Cr(alloy) \quad (1)$$

Reaction (1) implies that the noble metal atoms formed by reduction of the transient oxide dissolves back into the alloy. However, the present observation of Fe- and Cr- rich nanoparticles, which are substoichiometric with respect to oxygen (See Table 1; Fig. 3), indicates that the reduction of the oxides of Fe and Cr by the

alloy may instead result in a dispersion of sub-stoichiometric nanoparticles in the oxide scale.

According to the APT analysis, the oxygen- poor nanoparticles are made up of a mixture of oxygen, aluminium, chromium and/or iron. One interpretation may be that this corresponds to a mixture of alumina and elemental Cr and/or Fe. However, at this point the available information does not allow us conclude on the precise nature of the oxygen-poor nanoparticles.

The APT analysis indicates a variation in composition within the band of nanoparticles. Thus, in the lower part of the band we find the fully oxidized Cr-rich nanoparticles together with the oxygen poor nanoparticles containing Cr but no Fe. In contrast, the oxygen poor nanoparticles containing Fe are found in the middle part of the nanoparticle band. This layering is attributed to a corresponding compositional gradient in the transient oxide, the Fe content decreasing and the Al content increasing with the distance to the oxide/gas interface. Similar gradients in the transient oxide have been reported for a FeCrAl alloys after oxidation in air at 600 and 700 °C [19]. The gradient is suggested to be caused by a gradual decrease in oxygen activity at the scale/alloy interface, implying that this part of the scale (corresponding to the transient oxide) has grown inward (Fig. 4).

As noted above, the lower part of the nanoparticle band contains fully oxidized ($(Al,Cr)_2O_3$) nanoparticles (Fig. 3c). It is suggested that these particles correspond to Cr-rich transient oxide that has not undergone reaction (1), presumably because it has become separated from the alloy by the inward-growing alumina layer. The irregular shape of the ($(Al,Cr)_2O_3$) nanoparticles suggests that they are isostructural with corundum and develop epitaxial relationships with the alumina matrix. As was already noted, the alumina closest to the alloy substrate is free from nanoparticles as well as containing very little dissolved Cr and Fe and is considered to have formed by inward diffusion of oxygen ions.

While the present paper concerns the scale microstructure after 1 h, it is worthwhile to discuss the consequences of the oxygen-poor Fe- and Cr-rich nanoparticles for the further development of the alumina scale. It is considered that with time, the oxygen-poor nanoparticles in the scale will become fully oxidized. In a Wagner oxidation scenario the Fe^{2+} and Cr^{3+} ions so formed would tend to migrate towards the scale/gas interface, leaving behind pores in the alumina matrix. This is expected to affect the Fe-rich particles in particular because Fe^{2+} is reported to have a higher mobility than Cr^{3+} in oxides [20] and because it is highly soluble in transient aluminas (e.g., γ-Al_2O_3). It is suggested that this may explain the pores often observed in the middle part of the alumina scales formed on FeCrAl alloys [1, 3].

Cr segregation is considered to influence ion transport along these oxide grain boundaries, which are located at the outward growing part of the oxide scale. However, when the inner α-Al_2O_3 scale grows thicker, ion transport along boundaries in the inward growing part becomes rate determining. Therefore, Cr segregated boundaries exert strong influence at the very early stage of oxidation. The influence weakens with the growth of inwards growing α-Al_2O_3.

Conclusions

HAADF imaging and APT were used to analyse the microstructure of the alumina scale formed on the commercial FeCrAl alloy, Kanthal APMT, at 900 °C after 1-hour exposure. The detailed information by APT shed new lights on the initial oxidation of FeCrAl alloys. For the first time Cr segregation to some of the Al_2O_3 grain boundaries was observed. The continuous Cr-rich band, which contains a large number of Cr- and/or Fe- enriched nano-sized particles, was studied in detail. Four types of nanoparticles were found. Three types are nanoparticles with different ratio of Cr and Fe and a spheroid-shape. And they are the products of the reduction process to relatively noble metal by Al_2O_3. The fourth type is supersaturated solid solution of $((Al,Cr)_2O_3$ particles with an irregular shape. They will finally be transformed into thermodynamically more stable metal.

Acknowledgments We are grateful to the Swedish Research Council to provide financial support to acquire the atom probe tomography instrument. This work was carried out within the Swedish High Temperature Corrosion Centre (HTC). Fang Liu are grateful to Professors Krystyna Stiller and Hans-Olof Andrén, and Dr Mattias Thuvander for fruitful discussion.

References

1. F. Liu, H. Götlind, J.-E. Svensson, M. Halvarsson and L.-G. Johansson, Early stages of the oxidation of a FeCrAlRE alloy (Kanthal AF) at 900°C; a detailed microstructural investigation. *Corrosion Science* **50**, 2008 (2272–2281).
2. F. Liu, H. Gotlind, J. E. Svensson, L. G. Johansson and M. Halvarsson, TEM Investigation of the Microstructure of the Scale Formed on a FeCrAlRE Alloy at 900 A degrees C: The Effect of Y-rich RE Particles. *Oxidation of Metals* **74**, 2010 (11–32).
3. F. Liu, H. Josefsson, J.-E. Svensson, M. Halvarsson and L.-G. Johansson, TEM investigation of the oxide scales formed on a FeCrAlRE alloy (Kanthal AF) at 900°C in dry O_2 and O2 with 40% H_2O. *Materials at High Temperatures* **22**, 2005 (521–526).
4. F. Liu, H. Josefsson, J.-E. Svensson, M. Halvarsson, L.-G. Johansson, SEM investigation of reactive element particles on the surface of Kanthal AF oxidized at 900°C. In: 16th International Corrosion Congress, Beijing China, pp. Paper 19–22 (2005).
5. R. Cueff, H. Buscail, E. Caudron, C. Issartel and F. Riffard, Oxidation of alumina formers at 1173 K: effect of yttrium ion implantation and yttrium alloying addition. *Corrosion Science* **45**, 2003 (1815–1831).
6. J. Engkvist, S. Canovic, F. Liu, H. Götlind, J.-E. Svensson, L.-G. Johansson, M. Olsson and M. Halvarsson, Oxidation of FeCrAl foils at 500–900°C in dry O_2 and O_2 with 40% H_2O. *Materials at high Temperatures* **26**, 2009 (199–210).
7. D. A. Muller, Structure and bonding at the atomic scale by scanning transmission electron microscopy. *Nature Materials* **8**, 2009 (263–270).
8. E. A. Marquis, N. A. Yahya, D. J. Larson, M. K. Miller and R. I. Todd, Probing the improbable: imaging C atoms in alumina. *Materials Today* **13**, 2010 (34–36).
9. G. Sundell, M. Thuvander and H. O. Andren, Enrichment of Fe and Ni at metal and oxide grain boundaries in corroded Zircaloy-2. *Corrosion Science* **65**, 2012 (10–12).
10. K. Stiller, L. Viskari, G. Sundell, F. Liu, M. Thuvander, H. O. Andren, D. J. Larson, T. Prosa and D. Reinhard, Atom Probe Tomography of Oxide Scales. *Oxidation of Metals* **79**, 2013 (227–238).
11. S. Lozano-Perez, D. W. Saxey, T. Yamada and T. Terachi, Atom-probe tomography characterization of the oxidation of stainless steel. *Scripta Materialia* **62**, 2010 (855–858).
12. D. J. Young, T. D. Nguyen, P. Felfer, J. Zhang and J. M. Cairney, Penetration of protective chromia scales by carbon. *Scripta Materialia* **77**, 2014 (29–32).
13. F. Liu and K. Stiller, Atom probe tomography of thermally grown oxide scale on FeCrAl. *Ultramicroscopy* **132**, 2013 (279–284).

14. J. E. Tang, F. Liu, H. Asteman, J.-E. Svensson, L.-G. Johansson and M. Halvarsson, Investigation of FIB-thinned TEM cross-sections of oxide scales formed on type 310 steel at 600°C in water vapour-containing oxygen atmospheres. *Materials at High Temperatures* **24**, 2007 (27–55).
15. F. Liu, D. H. R. Fors, A. Golpayegani, H.-O. Andrén and G. Wahnström, Effect of boron on carbide coarsening at 600°C in 9–12% chromium steels. *Metallurgical and materials Transactions A-Physical Metallurgy and Materials Science* **43**, 2012 (4053–4062).
16. H. Götlind, F. Liu, J.-E. Svensson, M. Halvarsson and L.-G. Johansson, The effect of water vapour on initial stages of oxidation of the FeCrAl alloy Kanthal AF at 900°C. *Oxidation of Metals* **67**, 2007 (251–266).
17. M. Kusunoki, M. Rokkaku and Y. Ikuhara, TEM study on stability of Mg-doped gamma alumina fine particles. *Materials Transactions JIM* **39**, 1998 (110–113).
18. P. Kofstad, *High Tempertaure Corrosion*, (Elsevier Applied Science, London, 1988), pp. 342–388.
19. H. Josefsson, F. Liu, J.-E. Svensson, M. Halvarsson and L.-G. Johansson, Oxidation of FeCrAl alloys at 500–900°C in dry O_2. *Materials and Corrosion* **56**, 2005 (801–805).
20. J. Töpfer, S. Aggarwal and R. Dieckmann, Point defects and cation tracer diffusion in $(Cr_xFe_{1-x})_3 - \delta O_4$ spinels. *Solid State Ionics* **81**, 1995 (251–266).